Topological Hopf and Chain Link Semimetal States and Their Application to Co$_2$MnGa

Guoqing Chang,[1,2] Su-Yang Xu,[3,*] Xiaoting Zhou,[1,2] Shin-Ming Huang,[4] Bahadur Singh,[1,2]
Baokai Wang,[5] Ilya Belopolski,[3] Jiaxin Yin,[3] Songtian Zhang,[3] Arun Bansil,[5]
Hsin Lin,[1,2,†] and M. Zahid Hasan[3,6,‡]

[1]*Centre for Advanced 2D Materials and Graphene Research Centre, National University of Singapore,
6 Science Drive 2, Singapore 117546, Singapore*
[2]*Department of Physics, National University of Singapore, 2 Science Drive 3, Singapore 117542, Singapore*
[3]*Laboratory for Topological Quantum Matter and Spectroscopy (B7), Department of Physics, Princeton University,
Princeton, New Jersey 08544, USA*
[4]*Department of Physics, National Sun Yat-sen University, Kaohsiung 804, Taiwan*
[5]*Department of Physics, Northeastern University, Boston, Massachusetts 02115, USA*
[6]*Lawrence Berkeley National Laboratory, Berkeley, California 94720, USA*

Topological semimetals can be classified by the connectivity and dimensionality of the band crossings in momentum space. The band crossings of a Dirac, Weyl, or an unconventional fermion semimetal are zero-dimensional (0D) points, whereas the band crossings of a nodal-line semimetal are one-dimensional (1D) closed loops. Here we propose that the presence of perpendicular crystalline mirror planes can protect three-dimensional (3D) band crossings characterized by nontrivial links such as a Hopf link or a coupled chain, giving rise to a variety of new types of topological semimetals. We show that the nontrivial winding number protects topological surface states distinct from those in previously known topological semimetals with a vanishing spin-orbit interaction. We also show that these nontrivial links can be engineered by tuning the mirror eigenvalues associated with the perpendicular mirror planes. Using first-principles band structure calculations, we predict the ferromagnetic full Heusler compound Co$_2$MnGa as a candidate. Both Hopf link and chainlike bulk band crossings and unconventional topological surface states are identified.

Since the discovery of Dirac and Weyl semimetals [1–20], topological semimetals have emerged as an active frontier in condensed matter physics. Their unique topological properties are predicted to give rise to a wide range of exotic transport and optical phenomena [21–37]. By considering various rotational and mirror symmetries in both symmorphic and nonsymmorphic contexts, researchers have predicted nodal-line semimetals [38], higher charge double Weyl states [39,40], eightfold-degenerate double Dirac fermions [41], nonsymmorphic nodal-chain metals [42], the single threefold- and doubled sixfold-degenerate spin-1 Weyl points [43], nexus fermions [44–46], Kramers Weyl fermions [47], and magnetic Dirac semimetals [48–50]. Despite this diversity, topological semimetals can be further classified and characterized by the dimensionality of their band crossings in the bulk Brillouin zone (BZ). In a Dirac or Weyl semimetal or an unconventional (higher-fold degenerate) fermion semimetal [41,43–46], the conduction and valence bands cross at discrete points in the BZ. Therefore, the dimension of their band crossings is 0D. In a nodal-line semimetal [38], the conduction and valence bands touch along a closed loop; thus, the dimension of its band crossing is 1D. In this Letter, we propose a number of previously unidentified topological semimetals and identify a candidate material class for the experimental realization. They feature 3D band

crossings characterized by nontrivial links such as a Hopf link or a coupled chain enabled by perpendicular mirror planes. The Hopf link, which consists of two rings that pass through the center of each other, represents the simplest topologically nontrivial link. While originally studied in mathematics and other areas, recently, researchers have applied this concept to topological physics in order to construct novel topological insulators and superconductors [51–53], although the role of the Hopf link is distinctly different from what is considered here. Here we apply this idea to metals and show that the concept of the Hopf link can give rise to exotic, previously uncharacterized topological semimetals. We show that these nontrivial links can be identified by engineering the mirror eigenvalues of the conduction and valence bands on the two perpendicular mirror planes. We theoretically identify the ferromagnetic full Heusler compounds Co$_2$MnGa (Co$_2$MnAl) as candidates to experimentally realize this novel state of matter.

We start by considering a time-reversal breaking system with one mirror plane. The breaking of time-reversal symmetry makes all bands singly degenerate. If two inverted bands have opposite mirror eigenvalues, then their crossings on the mirror plane would be protected. This leads to a mirror-protected nodal line, as proposed in HgCr$_2$Se$_4$ [39], PbTaSe$_2$ [54], and ZrPtGe [55]. For two perpendicular mirror planes, the normal case would be two
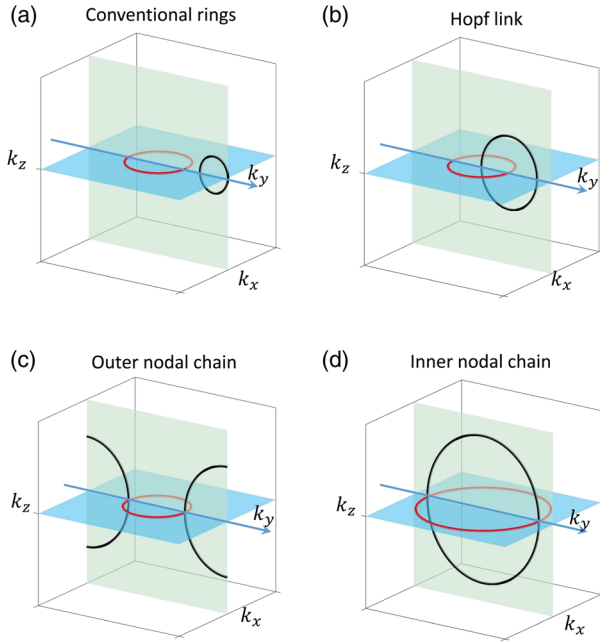
FIG. 1.   A variety of new topological semimetals characterized by 3D nontrivial links. (a) Two independent nodal lines protected by two perpendicular mirror planes. (b) When each nodal line passes through the center of the other, the two nodal lines form a nontrivial structure, a Hopf link. A Hopf link is a 3D structure which cannot be mapped to any 2D surface. (c),(d) When the two nodal lines touch at a point, they form a chain. When the two nodal lines are on opposite (same) sides of the touching point, they form an outer (inner) nodal chain.

unrelated nodal lines on the two mirrors [Fig. 1(a)]. However, there are more exotic cases [Figs. 1(b)–1(d)]. Specifically, a nodal chain consists of two perpendicular nodal lines that touch only at a point [Figs. 1(c) and 1(d)]. A Hopf link consists of two perpendicular nodal lines that hook each other.

In order to understand the symmetries and topological properties of these nontrivial links, it is helpful to study the line at which the two mirror planes coincide, i.e., the k_y axis in our schematics. We consider the situation in the absence of spin-orbit coupling (SOC). In this case, the states are segregated into the majority spin and the minority spin that do not hybridize with each other. Only time-reversal symmetry can translate between a majority spin state and a minority spin state. By contrast, spatial symmetries (space inversion, mirror, etc.) do not act on spins. Therefore, for the states of one spin (majority or minority), all crystalline symmetries are preserved [56]. The effect of SOC in the real material will be discussed later. Theoretical analysis indicates that the Hopf link proteced by the mirror symmetry requires four bands. On the k_y axis, these bands are described by a pair of indices, i.e., the eigenvalues of $\mathcal{M}_x$ and $\mathcal{M}_z$. As we scan along the k_y axis [Figs. 2(a) and 2(b)], we expect to encounter four crossings at the Fermi level. These four crossings divide the k_y axis into five regions, I–V.

Regions I and V are technically the same region due to periodicity. Starting from region I, we assume that the four bands have mirror eigenvalues of $[+, +]$ (red), $[-, +]$ (blue), $[-, -]$ (black), and $[-, +]$ (blue), respectively, as one decreases the energy. As we go from region I to region II, we encounter the first band crossing, where the $\mathcal{M}_x$ eigenvalue remains the same whereas the $\mathcal{M}_z$ eigenvalue flips. Another way to describe the same phenomena is to define a set of $\mathcal{Z}$ numbers $[\mathcal{Z}_x, \mathcal{Z}_z]$ for the two VBs, which describes the number of VBs with a positive mirror eigenvalue (+) on the $\mathcal{M}_x$ ($\mathcal{M}_z$) plane. For example, in region I, the two VBs are $[-, -]$ (black) and $[-, +]$ (blue). Therefore, the $\mathcal{Z}$ numbers are $[0, 1]$. In region II, the $\mathcal{Z}$ numbers become $[0, 2]$. Following this construction, we obtain the $\mathcal{Z}$ numbers of the two VBs at other regions, as labeled by the purple indices in Fig. 2(a). Notably, for the nontrivial Hopf link [Fig. 2(b)], while the $\mathcal{Z}$ numbers in regions I, II, IV, and V are identical to the case of two independent nodal lines [Fig. 2(a)], region III is different.
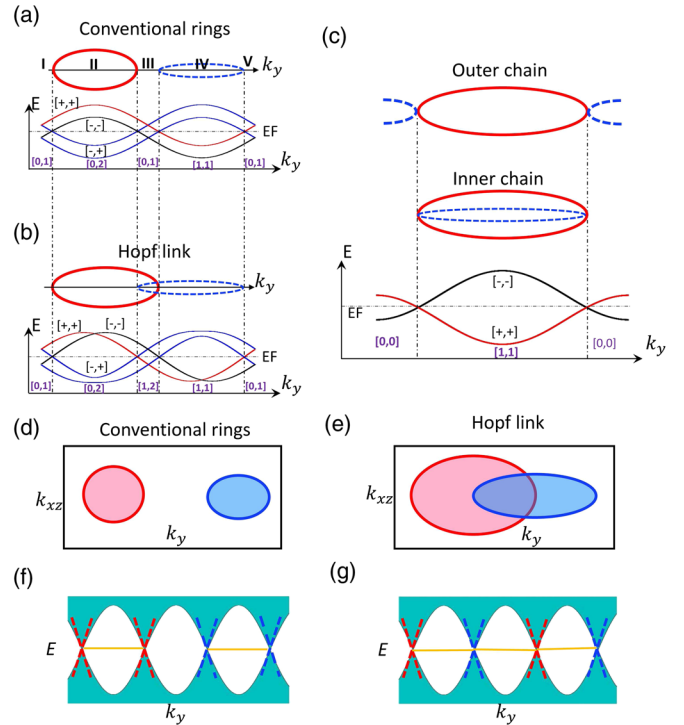

FIG. 2.   Mirror eigenvalues and topological surface states. (a) Two independent nodal lines (red and blue) on two perpendicular mirror planes (M_z and M_x). The panel below shows the mirror eigenvalues ($[M_x, M_z]$) of the VBs and CBs along the k_y axis. We also define a set of $\mathcal{Z}$ numbers $[\mathcal{Z}_x, \mathcal{Z}_z]$ for the two VBs. $\mathcal{Z}_x$ ($\mathcal{Z}_z$) describes the number of VBs with a positive mirror eigenvalue (+) on the $\mathcal{M}_x$ ($\mathcal{M}_z$) plane. (b),(c) The same as (a) but for a Hopf link (b) and an outer or inner nodal chain (c). (d),(e) Surface projections of two independent nodal lines (d) and a Hopf link (e). (f) Independent topological drum-head topological surface states of the two independent nodal lines. (g) Coupled topological drum-head surface states of a Hopf link.

The different $\mathcal{Z}$ numbers in region III demonstrate that the two independent nodal lines [Fig. 2(a)] and the Hopf link are topologically distinct. In order to change from one to the other, one needs to invert both $\mathcal{M}_x$ and $\mathcal{M}_z$ eigenvalues between the conduction bands (CBs) and valence bands (VBs) in this region.

In contrast to the Hopf link, our nodal chains on perpendicular mirror planes involve only two bands. As shown in Fig. 2(c), two band crossings divide the k_y axis into two regions under a periodic boundary condition. Interestingly, for nodal chains, both mirror eigenvalues ($\mathcal{M}_x$ and $\mathcal{M}_z$) flip from one region to the other. As a result, both $\mathcal{Z}$ numbers change [e.g., from [0, 0] to [1, 1] in Fig. 2(c)]. In a Hopf link, only one $\mathcal{Z}$ number changes from one region to the adjacent one. This difference highlights the topological distinction between a Hopf link and a nodal chain on perpendicular mirror planes.

We now consider the topological surface states. For a nodal line, its topological surface states have been established as the so-called drum-head surface states that fill the entire area inside the nodal line. This can be demonstrated by the nontrivial winding number. Essentially, the Berry phase of a k-space loop is $\pi(0)$ if the loop does (does not) enclose the nodal line [Figs. 2(d) and 2(f)]. By contrast, for a Hopf link, the surface projections of the two interlinked nodal lines overlap with each other [Fig. 2(e)]. The nontrivial winding number guarantees that each band crossing must be connected to a surface state. The topological surface states fill not only the areas owned by one of the nodal lines but also the area shared between the two nodal lines [Fig. 2(e)]. As a result, the two drum-head surface states are coupled together [Figs. 2(e) and 2(g)]. We emphasize that, in contrast to two independent nodal lines, the two nodal lines of a Hopf link must overlap when projected on the surface. As a result, a Hopf link's topological surface states always stitch the two interlinked nodal lines together.

We now present Co$_2$MnGa as a material candidate of the new topological semimetal state with nontrivial links. The full Heusler Co$_2$MnGa crystal structure has a face-centered cubic Bravais lattice, with space group $Fm\bar{3}m$ (No. 225) [57], and can be viewed as consisting of exactly four interpenetrating face-centered cubic lattices [Fig. 3(a)]. This crystal has many mirror planes including $\mathcal{M}_x$, $\mathcal{M}_y$, $\mathcal{M}_z$, $\mathcal{M}_{xy}$, $\mathcal{M}_{x\bar{y}}$, $\mathcal{M}_{xz}$, $\mathcal{M}_{x\bar{z}}$, $\mathcal{M}_{yz}$, and $\mathcal{M}_{y\bar{z}}$. Here the subscript index represents the out-of-plane direction of the mirror plane. xy means the direction that is 45° between $\hat{x}$ and $\hat{y}$. The Co$_2$MnGa samples are known to have a high Curie temperature (~700 K) and a collinear ferromagnetic order [58]. Figures 3(b) and 3(c) show the bulk band structure of the spin-up and spin-down states, respectively. Near the Fermi level, the spin-down states contribute a large holelike pocket at the BZ center Γ point. This pocket is relatively uninteresting from the topology point of view. We focus on the spin-up states, which show interesting
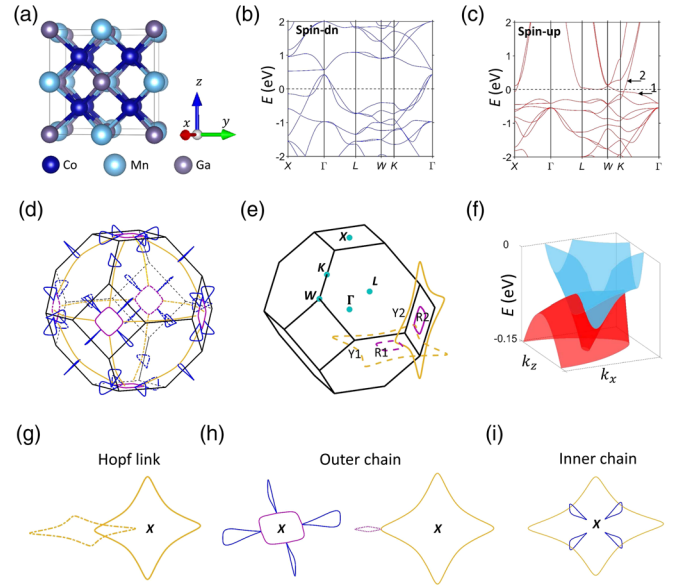

FIG. 3.   Hopf links and nodal chains in Co$_2$MnGa. (a) Crystal structure of Co$_2$MnGa. (b) Spin-down band structure. (c) Spin-up band structure. A band crossing is observed near the K point. (d) Band crossings between bands 1 and 2 all over the bulk BZ. Three types of nodal lines are observed, which are colored by blue, red, and yellow, respectively. The yellow and red nodal lines lie on the M_x, M_y, and M_z mirror planes. The blue nodal lines lie on the M_{xy}, $M_{x\bar{y}}$, M_{yz}, $M_{y\bar{z}}$, M_{xz}, and $M_{x\bar{z}}$ mirror planes. (e) The red and blue nodal lines at the corner of the Brillouin zone. Y1 and R1 (Y2 and R2) are located on the M_z (M_x) mirror plane. (f) 3D band structure ($E - k_x - k_z$) of a blue nodal line. (g)–(i) Decomposing the complicated nodal features into the basis units in Fig. 1. (g) Two yellow nodal lines form a Hopf link. (h) A blue nodal line and a red nodal line (or a yellow and a red nodal line) form an outer nodal chain. (i) A blue nodal line and a yellow nodal line form an inner nodal chain.

band crossings near the BZ boundaries between the lowest lying CB and VB [bands 1 and 2 in Fig. 3(c)]. Figure 3(d) depicts all the band crossings between bands 1 and 2 in the bulk BZ. We found three kinds of nodal lines, which are shown in red, yellow, and blue, respectively. Both the yellow and blue nodal lines are protected by the $\mathcal{M}_x$, $\mathcal{M}_y$, and $\mathcal{M}_z$ mirror planes, whereas the blue ones are protected by $\mathcal{M}_{xy}$, $\mathcal{M}_{x\bar{y}}$, $\mathcal{M}_{xz}$, $\mathcal{M}_{x\bar{z}}$, $\mathcal{M}_{yz}$, and $\mathcal{M}_{y\bar{z}}$. Remarkably, all these nodal lines are interconnected. We decompose such a complex nodal network into the basic units described in Fig. 1. As shown in Figs. 3(e) and 3(g), two yellow nodal lines are interlinked, forming a Hopf link. Each yellow nodal line is also connected to four red ones to form an outer nodal chain [Figs. 3(e) and 3(h)]. Moreover, each red nodal line is further connected to four blue ones to form an outer nodal chain. Furthermore, each yellow nodal line is connected to four blue ones to form an inner nodal chain. Therefore, all nontrivial links described in Figs. 1 and 2 are realized in Co$_2$MnGa. We have built a six-band tight-binding model that reproduces all the band crossings in
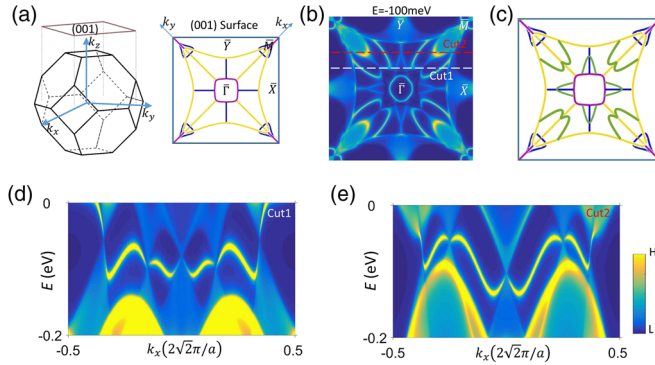
FIG. 4.   Drum-head topological surface states in Co_2MnGa. (a) The bulk BZ and the projection of all nodal features onto the (001) surface. (b) Surface states with Co termination at 100 meV below the Fermi level. The sharp features are surface states, whereas the shaded region are projections of bulk bands. (c) Schematic illustration of the surface state connectivity observed in (b). The green curves represent the surface states, whereas other lines are the projections of the bulk nodal lines as in (a). (d),(e) Energy dispersions along the white and red cuts indicated in (c). Surface states connecting adjacent band crossings are observed.

Co_2MnGa. The detailed model is shown in Supplemental Material [59]. We have further calculated the band structure with an on-site Coulomb repulsion U. We found that the band crossing is robust against on-site Coulomb repulsion U, while its energy may shift with respect to the Fermi level (Fig. S5). In the main text, we chose $U = 0$ as the calculated magnetic moment, for $U = 0$ matches the best with the experimentally observed value [58]. Now we consider the effects of SOC. The inclusion of SOC couples the two spins and allows them to hybridize. Therefore, the degree of mirror symmetry breaking due to SOC can be directly measured by the SOC gap opened at the band crossings. From first-principles calculations, we found that the SOC gap opened at the nodal links in Co_2MnGa is extremely small (<1 meV; see Fig. S4). Therefore, the SOC effect is quite small. In other words, the effect of mirror symmetry breaking due to spin orientations is negligible. Similar phenomena have also been found in other full Heusler compounds [56,65].

Finally, we show the calculated surface band structure of Co_2MnGa. We observe an ω-shaped surface state at the midpoint along each $\bar{\Gamma} - \bar{M}$ and a V-shaped surface state along each $\bar{\Gamma} - \bar{X}$ line. As we travel across the surface BZ along the red (white) dotted line across the surface BZ, we expect to cross the nodal lines five times. Indeed, we found five band crossings in Figs. 4(d) and 4(e). Importantly, all surface states are found to connect the adjacent band crossings. Based on Figs. 4(b), 4(d), and 4(e), we conclude that the ω-shaped surface states connect two yellow nodal lines [in Fig. 4(b), one straight yellow line along $45°$ and the other curved yellow line that form a large closed loop], while the V-shaped surface state connect a blue nodal line

with the red nodal line at $\bar{\Gamma}$. The two yellow nodal lines form a Hopf link [Fig. 3(g)]. The blue and red nodal lines form an outer nodal chain [Fig. 3(h)]. The ω-shaped and the V-shaped surface states are the topological surface states. Topological surface states connecting other nontrivial links can also be identified at other binding energies.

Note added.—Recently, we noticed two independent works [66,67] that also proposed the Hopf-link semimetal concept. Despite some similarity, our work is unique and distinct in two ways: (i) We consider the Hopf link and nodal chains enabled by a perpendicular mirror plane mechanism; (ii) crucially, we also identify a material candidate which will open the experimental front for Hopf-link materials research.

[*]suyangxu@princeton.edu
[†]nilnish@gmail.com
[‡]mzhasan@princeton.edu
[1] H. Weyl, Z. Phys. **56**, 330 (1929).
[2] C. Herring, Phys. Rev. **52**, 365 (1937).
[3] G. E. Volovik, *The Universe in a Helium Droplet* (Oxford University, New York, 2003).
[4] S. Murakami, New J. Phys. **9**, 356 (2007).
[5] X. Wan, A. M. Turner, A. Vishwanath, and S. Y. Savrasov, Phys. Rev. B **83**, 205101 (2011).
[6] A. A. Burkov and L. Balents, Phys. Rev. Lett. **107**, 127205 (2011).
[7] M. Z. Hasan, S.-Y. Xu, I. Belopolski, and S.-M. Huang, Annu. Rev. Condens. Matter Phys. **8**, 289 (2017).
[8] N. P. Armitage, E. J. Mele, and A. Vishwanath, arXiv:1705.01111.
[9] A. Bansil, H. Lin, and T. Das, Rev. Mod. Phys. **88**, 021004 (2016).
[10] Z. Wang, Y. Sun, X. Q. Chen, C. Franchini, G. Xu, H. Weng, X. Dai, and Z. Fang, Phys. Rev. B **85**, 195320 (2012).
[11] Z. K. Liu *et al.*, Science **343**, 864 (2014).

[12] S.-Y. Xu *et al.*, Science **347**, 294 (2015).
[13] M. Neupane *et al.*, Nat. Commun. **5**, 3786 (2014).
[14] S. Borisenko, Q. Gibson, D. Evtushinsky, V. Zabolotnyy, B. Buchner, and R. J. Cava, Phys. Rev. Lett. **113**, 027603 (2014).
[15] Z. K. Liu *et al.*, Nat. Mater. **13**, 677 (2014).
[16] S. M. Huang *et al.*, Nat. Commun. **6**, 7373 (2015).
[17] H. Weng, C. Fang, Z. Fang, B. A. Bernevig, and X. Dai, Phys. Rev. X **5**, 011029 (2015).
[18] S.-Y. Xu *et al.*, Science **349**, 613 (2015).
[19] L. Lu, Z. Wang, D. Ye, L. Ran, L. Fu, J. D. Joannopoulos, and M. Soljačić, Science **349**, 622 (2015).
[20] B. Q. Lv *et al.*, Phys. Rev. X **5**, 031013 (2015).
[21] M. Z. Hasan and C. L. Kane, Rev. Mod. Phys. **82**, 3045 (2010).
[22] X.-L. Qi and S.-C. Zhang, Rev. Mod. Phys. **83**, 1057 (2011).
[23] H. B. Nielsen and M. Ninomiya, Phys. Lett. B **130**, 389 (1983).
[24] S. A. Parameswaran, T. Grover, D. A. Abanin, D. A. Pesin, and A. Vishwanath, Phys. Rev. X **4**, 031035 (2014).
[25] A. C. Potter, I. Kimchi, and A. Vishwanath, Nat. Commun. **5**, 5161 (2014).
[26] Y. Baum, E. Berg, S. A. Parameswaran, and A. Stern, Phys. Rev. X **5**, 041046 (2015).
[27] K. Taguchi, T. Imaeda, M. Sato, and Y. Tanaka, Phys. Rev. B **93**, 201202(R) (2016).
[28] H. Ishizuka, T. Hayata, M. Ueda, and N. Nagaosa, Phys. Rev. Lett. **117**, 216601 (2016).
[29] I. Sodemann and L. Fu, Phys. Rev. Lett. **115**, 216806 (2015).
[30] C.-K. Chan, N. H. Lindner, G. Refael, and P. A. Lee, Phys. Rev. B **95**, 041104 (2017).
[31] T. Morimoto, S. Zhong, J. Orenstein, and J. E. Moore, Phys. Rev. B **94**, 245121 (2016).
[32] F. de Juan, A. G. Grushin, T. Morimoto, and J. E. Moore, arXiv:1611.05887.
[33] C.-K. Chan, P. A. Lee, K. S. Burch, J. H. Han, and Y. Ran, Phys. Rev. Lett. **116**, 026805 (2016).
[34] Y. Chen, S. Wu, and A. A. Burkov, Phys. Rev. B **88**, 125105 (2013).
[35] P. Hosur and X.-L. Qi, Phys. Rev. B **91**, 081106(R) (2015).
[36] P. Goswami, G. Sharma, and S. Tewari, Phys. Rev. B **92**, 161110(R) (2015).
[37] J. Ma and D. A. Pesin, Phys. Rev. B **92**, 235205 (2015).
[38] C. Fang, H. Weng, X. Dai, and Z. Fang, Chin. Phys. B **25**, 117106 (2016).
[39] C. Fang, M. J. Gilbert, X. Dai, and B. A. Bernevig, Phys. Rev. Lett. **108**, 266802 (2012).
[40] S.-M. Huang *et al.*, Proc. Natl. Acad. Sci. U.S.A. **113**, 1180 (2016).

[41] B. J. Wieder, Y. Kim, A. M. Rappe, and C. L. Kane, Phys. Rev. Lett. **116**, 186402 (2016).
[42] T. Bzdušek, Q. Wu, A. Rüegg, M. Sigrist, and A. A. Soluyanov, Nature (London) **538**, 75 (2016).
[43] B. Bradlyn *et al.*, Science **353**, 6299 (2016).
[44] G. Chang *et al.*, Sci. Rep. **7**, 1688 (2017).
[45] H. Weng, C. Fang, Z. Fang, and X. Dai, Phys. Rev. B **93**, 241202 (2016).
[46] Z. Zhu, G. W. Winkler, Q. S. Wu, J. Li, and A. A. Soluyanov, Phys. Rev. X **6**, 031003 (2016).
[47] G. Chang *et al.*, arXiv:1611.07925.
[48] P. Tang, Q. Zhou, G. Xu, and S.-C. Zhang, Nat. Phys. **12**, 1100 (2016).
[49] S. M. Young and B. Wieder, arXiv:1609.06738.
[50] J. Wang, Phys. Rev. B **95**, 115138 (2017).
[51] J. E. Moore, Y. Ran, and X.-G. Wen, Phys. Rev. Lett. **101**, 186805 (2008).
[52] R. Kennedy, Phys. Rev. B **94**, 035137 (2016).
[53] B. Lian, C. Vafa, F. Vafa, and S.-C. Zhang, Phys. Rev. B **95**, 094512 (2017).
[54] G. Bian *et al.*, Nat. Commun. **7**, 10556 (2016).
[55] B. Singh, X. Zhou, H. Lin, and A. Bansil, arXiv:1703.04048.
[56] Z. Wang, M. G. Vergniory, S. Kushwaha, M. Hirschberger, E. V. Chulkov, A. Ernst, N. P. Ong, R. J. Cava, and B. A. Bernevig, Phys. Rev. Lett. **117**, 236401 (2016).
[57] J. Kübler, G. H. Fecher, and C. Felser, Phys. Rev. B **76**, 024414 (2007).
[58] K. R. A. Ziebeck and K.-U. Neumann, *Alloys and Compounds of d-Elements with Main Group Elements* (Springer-Verlag, Berlin, 2001).
[59] See Supplemental Material at http://link.aps.org/supplemental/10.1103/PhysRevLett.119.156401 for further details, which includes Refs. [60–64].
[60] P. Hohenberg and W. Kohn, Phys. Rev. **136**, B864 (1964).
[61] G. Kresse and J. Furthmüller, Phys. Rev. B **54**, 11169 (1996).
[62] G. Kresse and D. Joubert, Phys. Rev. B **59**, 1758 (1999).
[63] J. P. Perdew, K. Burke, and M. Ernzerhof, Phys. Rev. Lett. **77**, 3865 (1996).
[64] P. J. Webster and K. R. A. Ziebeck, in *Alloys and Compounds of d-Elements with Main Group Elements. Part 2*, edited by H. R. J. Wijn, Landolt-Börnstein, New Series, Group III Vol. 19c (Springer, Berlin, 1988), pp. 75–184.
[65] G. Chang *et al.*, Sci. Rep. **6**, 38839 (2016).
[66] W. Chen, H.-Z. Lu, and J.-M. Hou, arXiv:1703.10886.
[67] Z. Yan, R. Bi, H. Shen, L. Lu, S.-C. Zhang, and Z. Wang, arXiv:1704.00655.